

Structural Performance of Connectors in a Hardwood Stairway Handrail Guard System

Franklin Quin, Jr.,^{a,*} Tamara Franca,^{a,*} Jason Street,^a Hyungsuk Lim,^b and Rubin Shmulsky^a

Wood is a preferred material for constructing staircases due to its appealing aesthetic features. The use of wood, especially hardwoods such as red oak (*Quercus rubra*), white oak (*Quercus alba*), yellow poplar (*Liriodendron tulipifera*), and hard maple (*Acer saccharum*), has been the main construction material for staircases over the years. Staircase designs have evolved because of the flexibility of wood and working with specialized manufacturing machinery. A stair guard system connection must be designed to resist rotational and translational movements whenever a force is applied to the handrail. The demand for structural design values in wooden stair guards has been steadily increasing, driven by the needs of engineers, designers, builders, and end-users alike. This paper presents experimental data for four stair guard connections (post-to-rail, infill-to-footing, infill-to-rail, and rail-to-rail) encountered in a hardwood stairway handrail guard system. The data generated from this research could be useful for modeling the structural behavior of the connections.

DOI: 10.15376/biores.19.1.1410-1432

Keywords: Hardwoods; Staircases; Stair guard connections; Rotational; Translational

Contact information: a: Department of Sustainable Bioproducts, Mississippi State University, Box 9820, Mississippi State, MS 39762; b: University of Canterbury, Christchurch, New Zealand;

* Corresponding authors: fq3@msstate.edu; tsf97@msstate.edu

INTRODUCTION

Staircases are a facet of societal existence, potentially posing considerable safety hazards when their design is not appropriately executed. Some of the major factors that influence stairway safety are variability in rise and run, stair steepness, and handrail design (Templer *et al.* 1985). The purpose of the handrail is to aid in preventing falls and the severity of falls on the staircase. Maki (1985) conducted a study illustrating the typical forces and moments individuals apply to a handrail while standing upright and holding onto it. These forces would escalate substantially in the event of preventing a fall, subjecting the staircase to considerably greater loads.

Most hardwood stairway guard components are manufactured according to traditional designs with dimensions and mechanical properties based on the experience of the stair builder. Stairways are often designed from an aesthetic point of view as compared to an engineering design view. The structural behavior of a stairway system can be simulated using a finite element (FE) model that considers stair components as simple beam elements (Pousette 2006).

The structural behavior of the stairway system is contingent upon the mechanical characteristics of the stairway guard components and the rigidity of their joints. The joints

between the post and handrail are usually assembled with different types of connectors, which can be also glued. There are certain variables that can be changed in this type of joint, such as the thickness of the rail, the size of the hole drilled in the rail or post, the dimensions of the fasteners, the stiffness of the connection, and the actual properties of the wood (Pousette 2006 and Pencik 2015). The literature states that a beam is a tri-dimensional member with one dimension significantly greater than the other two (Bauchau and Craig 2009). Based upon that assumption, the Euler-Bernoulli simple beam theory can be used to analyze the data (Bauchau and Craig 2009). The structural behavior of the stairway guard joints is characterized by their translational and rotational resistance, which is more challenging to simulate due to the complex interaction between their components such as threaded metal rods, washers, and profiled wood members.

As one of the main functionalities of a stairway guard system is fall prevention, the guard system's performance against out-of-plane loads needs to be ensured. Thus, the reference data on such structural performance is required to design the guard system in compliance with building codes. The building codes for staircases are described in the International Residential Code (IRC), under Section R311 for Means of Egress (International Code Council, 2017). The IRC lists a minimum and maximum handrail height of 34 in. and 38 in., respectively. According to ASCE/SEI 7-10-Minimum Design Loads for Building and Other Structures states that handrail and guardrail systems should be designed to "resist a single concentrated load of 200 pounds applied in any direction at any point along the top and to transfer this load through the supports to the structure" (American Society of Civil Engineers 2005). According to the American Society of Civil Engineers ASCE/SEI 7-10-Minimum Design Loads for Buildings and Other Structures states that panel fillers (assuming as balusters) should be able to resist a horizontally applied normal force of 50 pounds on an area not to exceed 12" x 12". The International Building Code states that balusters used for decks, the baluster must be able to sustain a minimum testing force of 50 pounds of concentrated load.

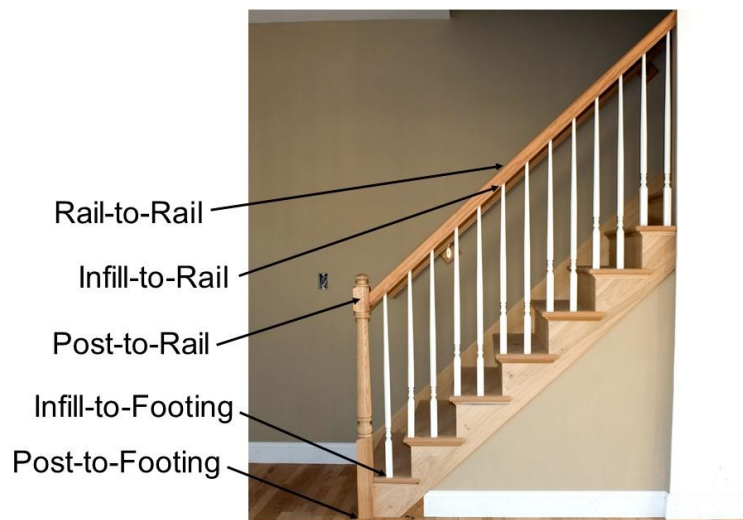


Fig. 1. Stair guard system (image downloaded from <http://www.storyblocks.com>)

The structural performance of stairway guard system wood members can be designed using the published values of the hardwood species commonly used for the guard

system construction (FPL 2021). However, the structural design of the guard system joints often is impractical due to their complex design without engineering data. Thus, this study aimed to evaluate the structural performance of four joint types that compose a common stair guard system: the post-to-rail, infill(baluster)-to-footing, infill(baluster)-to-rail, and the rail-to-rail connection (Fig. 1) (Wynne *et al.* 2000).

EXPERIMENTAL

Post-to-Rail

Wood species

Kiln-dried, defect-free, and straight-grained glue laminated red oak (*Quercus rubra*) rails (2 ½" x 1 ¾" x 45") and posts (3 ½" x 3 ½" x 44") used by staircase manufacturers were secured from Fitts Industries, Inc. in Tuscaloosa, AL. The average moisture content of the red oak specimens was 7.4%, as measured following ASTM D 4442 (ASTM 2020). The rails and posts were cut to size in the wood shop at the Department of Sustainable Bioproducts at Mississippi State University, Starkville, MS. The posts and rails were kept in a controlled environment (21 °C and 65% relative humidity (RH)) for several weeks until joint fabrication. Each joint specimen was identified by configuration number (C1 and C2), type of load applied (S for preliminary, M for monotonic, and C for reversed cyclic), and repetition number (1 to 5). For example, the third repetition, under monotonic load, for configuration #2 had the label C2-M-3.

Rail & post fastener #301 (configuration 1) (c1)

The rail & post fastener #301 (Fig. 2a) is widely used in the staircase industry to link posts to treads and/or rails. This connector is also typically used where a normal rail-bolt connector #302 (Fig. 3a) does not work. For the rail & post fastener #301, a 1" dia. x 2 ½" deep hole was drilled in the center of the wide face of the post. A 7/16" dia. hole was then drilled through the 1" hole in the post to the outside of the post. A ¼" dia. x 2" deep hole was drilled end-grain into the center cross-section of the rail. The 3/8" dia. lag screw was then inserted through the 7/16" dia. hole in the post and then screwed into the ¼" dia. hole in the rail with a socket wrench until the post was snug against the rail. Fig. 2b shows the rail & post fastener #301 configuration assembly.

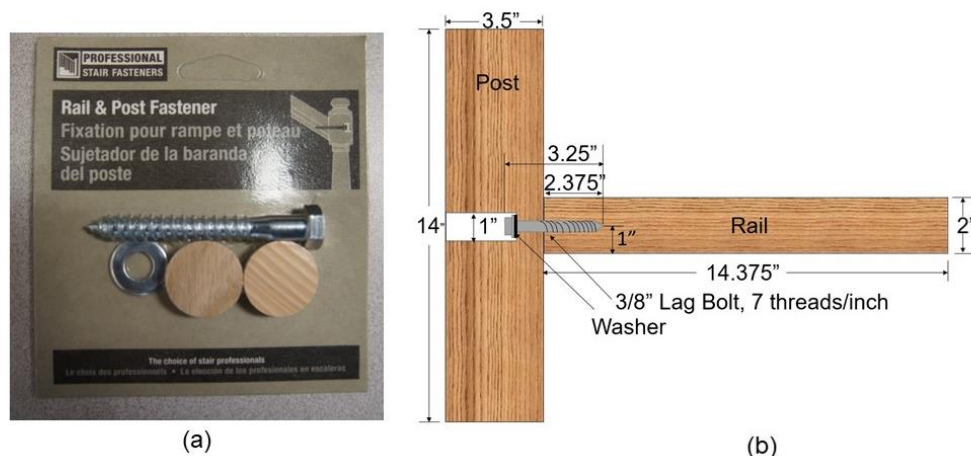


Fig. 2. (a) Rail & Post Fastener #301 (3/8" lag screw, 7 threads/inch) (b) Rail & Post Fastener #301 Joint

Rail-bolt fastener #302 (configuration 2) (c2)

The rail-bolt fastener #302 (Fig. 3a) is also commonly used to secure rails to posts. For the rail-bolt fastener #302, a ¼" dia. x 2" deep hole was drilled perpendicular to the grain into the center of the wide face of the post. The lag-screw thread end of the hanger bolt was inserted into the post with a rail-bolt wrench. A 3/8" dia. x 2" deep hole was drilled into the end-grain in the center cross-section of the rail, and a 1" dia. hole was drilled perpendicular to the grain 1 ½" from the end of the rail to a depth of 1 ½". A plastic washer was then inserted into the 1" hole in the rail. The rail was then inserted onto the machine-bolt thread end of the hanger bolt on the post through the 3/8" hole in the rail and through the plastic washer. A serrated flange metal nut was then inserted into the 1" hole in the rail and fastened to the machine end of the rail-bolt using the rail bolt wrench. Fig. 3b shows the rail-bolt fastener #302 configuration.

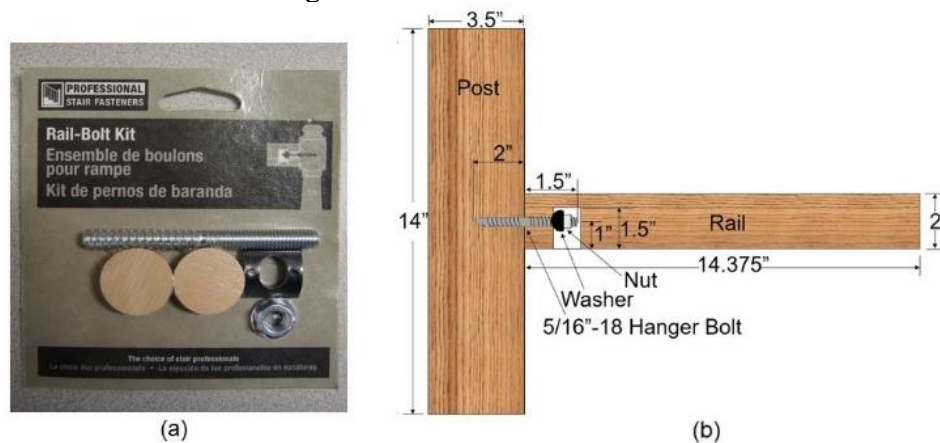


Fig. 3. (a) Rail-Bolt Fastener #302 (5/16-18 hanger bolt) (b) Rail-Bolt Fastener #302 Joint

Static loading protocol and measurements

The maximum moment carry capacity of the post-to-rail joints was evaluated by cantilever bending tests. These tests were conducted to find the reference maximum loads for the monotonic and cyclic tests. Ten joints (C1-S-1, C1-S-2, C1-S-3, C1-S-4, C1-S-5, C2-S-1, C2-S-2, C2-S-3, C2-S-4, C2-S-5) were tested. The bending moment arm was 12". Two linear variable differential transformers (LVDTs) were installed parallel to the rail for measuring the rail's rotational movement, as shown in Fig. 4a. The two parallel LVDTs were placed on top and bottom 3 ½" away from the post, rail's center. The distance between the LVDTs was 3 3/8". One wire string potentiometer located on the neutral axis of the rail 10" from the post was used to measure the rail displacement at 10" from the post. The joint rotation was measured in radians with equation 1:

$$\theta = \arctan ((y_t + y_b) / d) \quad (1)$$

where θ is joint rotation in radians, y_t is the displacement measured by the LVDT, y_b is the displacement measured by the bottom LVDT, and d is the distance between LVDTs (3 3/8"), respectively. The LVDTs were positioned 3 ¼" from the post on the top and bottom sides of the rail. The joints were tested until failure on a SATEC (Instron) Universal Testing Machine Model 8800 (Norwood, MA, USA) at a loading rate of 0.5 in/min. The load was applied perpendicular to the rail top, while the test specimen was horizontally placed on the machine testing bed. The post was secured to the machine testing bed with two 18" x 3.75" x 0.75" A36 steel plates and four 0.5" x 24" bolts.

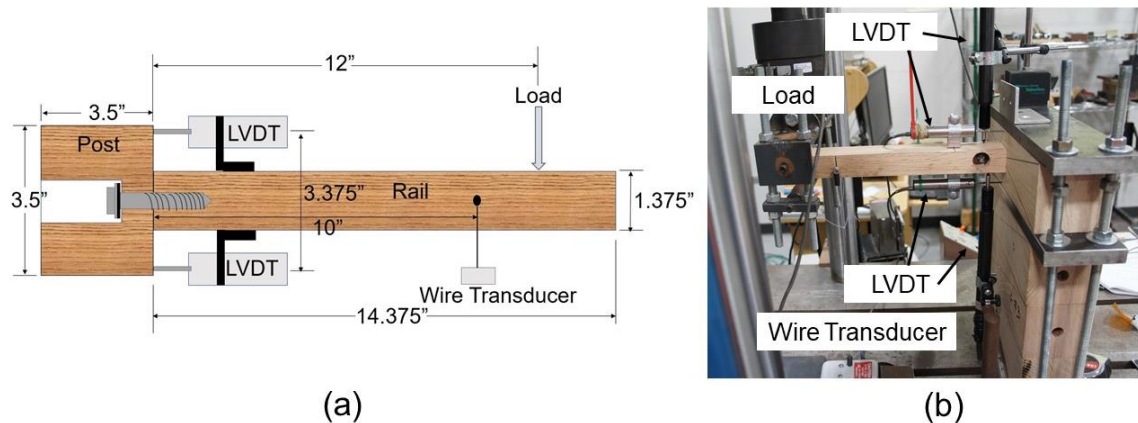


Fig. 4. (a) Simplified test setup along with instrumentation for measurements (b) test setup

Monotonic loading protocol and measurements

The monotonic tests were conducted based on the guidelines found in EN 26891:1991 (CEN 1991). The monotonic loading protocol has a force-control cycle and a displacement-control cycle. The maximum moment capacity of each joint configuration was determined in the preliminary loading tests. Ten joints (C1-M-1, C1-M-2, C1-M-3, C1-M-4, C1-M-5, C2-M-1, C2-M-2, C2-M-3, C2-M-4, C2-M-5) were tested. According to the standard, a moment is applied up to 40% of the estimated maximum moment-carrying capacity of the joint and maintained for 30 seconds. The moment is then reduced back to 10% of the estimated maximum moment capacity of the joint and maintained for 30 seconds. After this, the moment is increased to the ultimate maximum moment or a joint rotation of 0.15 rad. The loading rate below 70% of the estimated maximum moment capacity is 20% of the maximum moment per minute $\pm 25\%$. The loading rate above 70% is based upon a constant rate of joint rotation such that the ultimate moment or 0.15 rad joint rotation is reached in 3 to 5 minutes of additional testing time. The moment reached before (if there is a drop-in moment) or at a joint rotation of 0.15 rad, was recorded as the maximum for each specimen.

The curves generated from the monotonic load-displacement procedure found in EN 26891:1991 (CEN 1991) were used to define the initial stiffness (initial slip modulus) and maximum moment. The measurement of the yield moment, yield moment rotation, and ductility was taken from the procedure in EN 12512:2001 (CEN 2001).

Reversed-cyclic loading protocol and measurements

The reversed-cyclic tests were conducted based on the guidelines found in EN 12512:2001 (CEN 2001). The reversed-cyclic loading protocol is displacement-controlled based upon values obtained from the preliminary tests. Ten joints (C1-C-1, C1-C-2, C1-C-3, C1-C-4, C1-C-5, C2-C-1, C2-C-2, C2-C-3, C2-C-4, C2-C-5) were tested. A compressive load was gradually applied, reaching up to 25% of the estimated yield rotation for the joint calculated from the preliminary tests. Subsequently, the load was released, and the joint was subjected to a tension load until it reached zero rotation. Following this, a tensile load was incrementally imposed, reaching a magnitude of 25% of the projected yield rotation for the joint in tension. The joint was then unloaded, and a compressive load was reapplied to bring the joint back to zero rotation. This sequence constitutes the first cycle. The second cycle replicated the initial one, albeit with the applied loads progressing to 50% of the

estimated joint yield rotation. Subsequent cycles, namely the third, fourth, and fifth, were repetitions of the first cycle, but the applied loads reached 75% of the predicted joint yield rotation. The sixth, seventh, and eighth cycles similarly mirrored the first cycle, but with the applied loads reaching 100% of the estimated joint yield rotation. Beyond the eighth cycle, the pattern continued, occurring in sets of three cycles. These additional cycles corresponded to applied loads of 200%, 400%, 600%, and so forth, of the estimated joint yield rotation. The testing continued until the joint experienced failure or rotated to an angle of 0.15 radians. The reversed-cyclic loading was designed to achieve positive and negative displacements to mimic lateral displacement of the rail. The reversed cyclic hysteresis curves obtained by following the EN 12512:2001 (CEN 2001) loading protocol were used for reversed cyclic data analysis.

Infill(baluster)-to-Footing

Experiments were conducted on two infill-to-footing joint connection systems. The joints were constructed with red oak infills (baluster) and red oak footings (treads). The dimensions of the balusters were 1 1/4" x 1 1/4" x 14", while the dimensions of the footings were 5" x 16" x 1". Two different baluster fastener kit sizes were used. For the first baluster kit, a 3/16" x 1" hole was drilled into the bottom of the baluster. Subsequently, the fasteners were driven 1" into the baluster using a reversible drill. A 3/16" hole was then drilled in the center of the tread for the baluster to be hand-tightened onto the tread (see Fig. 5a). For the second baluster kit, a 9/32" x 1-1/4" hole was drilled into the bottom of the baluster. The fasteners were then drilled 1-1/4" into the baluster using a reversible drill. A 9/32" hole was then drilled in the center of the tread through the thickness.

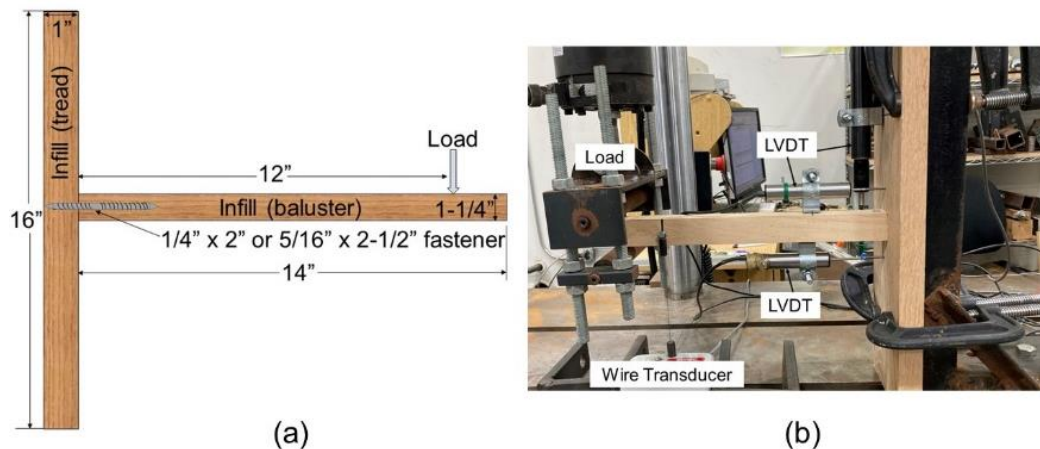


Fig. 5. (a) Baluster fastener kit joint (b) setup for testing infill-to-footing connection

The bending moment capacity of ten infill-to-footing joints was evaluated by cantilever bending tests. Five joints were constructed with the 1/4" x 2" baluster fastener, and five joints were constructed with the 5/16" x 2-1/2" baluster fastener. The moment arm for the testing was 12 inches. The cantilever test was used to estimate the maximum bending moment capacity and bending moment stiffness of the baluster fastener connector systems. Figure 5b shows the setup for the testing. Three LVDTs were used to measure the movement of the connection during testing. One LVDT was used to measure the translational movement of the baluster while two LVDTs were used to measure the rotation of the infill in reference to the footing. A wire string potentiometer was located 10" from

the joint connection to measure baluster movement 10" from the joint connection. The test loading rate was 0.5 in/min. The loading head used for the loading simulates a person's hand pushing outward against the baluster.

Infill(baluster)-to-Rail

Experiments were conducted on four configurations of infill-to-rail joint connections. The joints were constructed from red oak stair rails with dimensions of 2" x 1 3/8" x 14 3/8" and red oak infills (balusters) with dimensions of 1 1/4" x 1 1/4" x 14". The red oaks rails and balusters were donated by Fitts Industries, Tuscaloosa, AL. The rails and balusters were planned and cut to size in the wood shop at Mississippi State University, Department of Sustainable Bioproducts, Starkville, MS. The moisture content of the rails and the balusters were measured with a hand-held moisture meter to be approximately 10%. The ends of the balusters were cut at a 30° angle on a table saw. The ends of the balusters were connected to the rails with four 16-gauge finish nails and no glue or four 16-gauge finish nails with polyvinyl acetate (PVAC) glue. The 16-gauge finish nails were inserted through the balusters and into the rails with a Paslode Cordless XP 16-gauge Framing Nailer. Five joints were constructed with 16-gauge 1-1/4" nails and glue. Five joints were constructed with 16-gauge 1-1/2" nails and glue. Five joints were constructed with 16-gauge 1-1/4" nails and no glue. Five joints were constructed with 1-1/2" nails and no glue. Therefore, a total of twenty joints were tested. For the samples with glue, glue was only applied to one surface. The samples were conditioned indoors at 25.5°C and 49% relative humidity for approximately one week before testing. Figure 6a shows a diagram of the infill-to-rail joint that was tested.

The shearing strength of the infill-to-rail connection joints was evaluated from a double shear test when applying a distributed load across the middle span section of the infill (baluster) parallel to the connection joints of the infill-to-rail connection. The distributed load was applied through a 1" (thick) x 2" (wide) x 10" (length) metal block. Two linear variable differential transformers (LVDTs) were used to measure the joint movement at the two ends of the infill. The LVDTs were located at 0.5" from the rails on each end of the baluster. Figure 6b shows a diagram of the testing configuration for the infill-to-rail connections. The joints were secured to the testing frame with four C-clamps attached to the end of the rails. The test loading rate was 0.5 in/min.

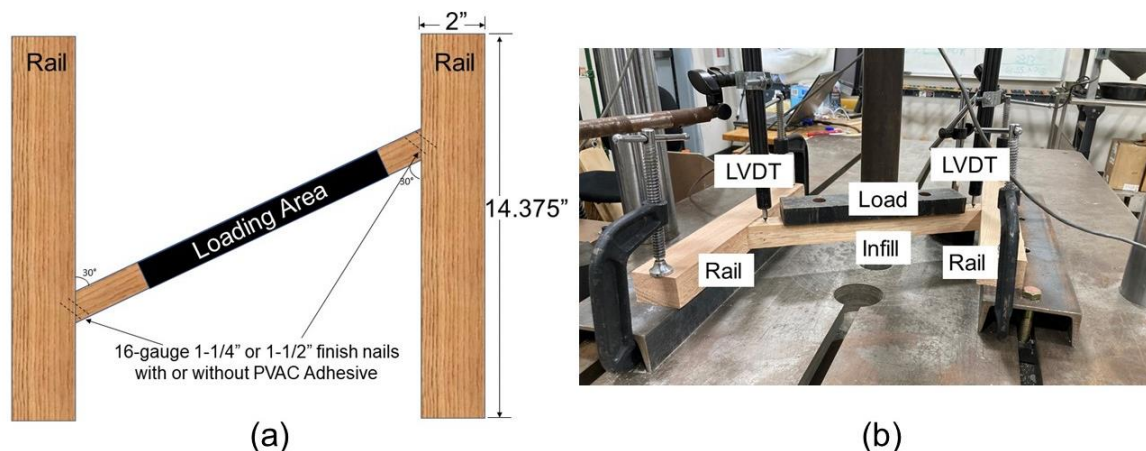


Fig. 6. (a) Infill-to-rail test joint (b) infill-to-rail test setup

Rail-to-Rail

Experiments were conducted on a rail-to-rail joint connection system. The joints were constructed from red oak rails with dimensions of 2" x 1 3/8" x 14 3/8". The connection system implemented was the rail-bolt kit fastener #302. For the rail-bolt fastener #302, a 1/4" x 2" deep hole was drilled into the center cross-section of one rail. The lag end of the bolt was inserted into the rail with a rail bolt wrench. On the other rail, a 3/8" x 2" deep hole was drilled into the center cross-section, and an additional 1" hole was created 1 1/2" from the rail's end, reaching a depth of 1.5". A plastic washer was then inserted into this 1" hole in the rail. The rail was inserted onto the rail bolt through the 3/8" hole in the rail. A metal nut was then inserted into the 1" hole in the rail and fastened to the machine end of the rail bolt using the rail bolt wrench. Figure 7a offers a visual representation of the tested joint. Fifteen rail-to-rail joints were constructed. In order to compare samples with a connector to a solid red oak rail without a joint, fifteen red oak rails were tested in static bending under the same loading conditions. Figure 7b illustrates the rail that underwent testing. A total of thirty test specimens were constructed.

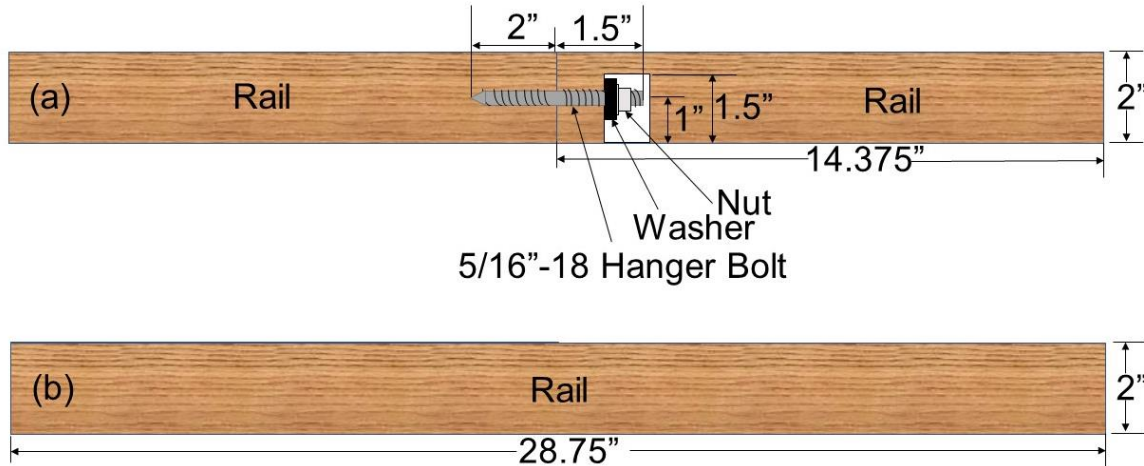


Fig. 7. (a) Rail-bolt fastener #302 joint (b) solid rail no mechanical fastener

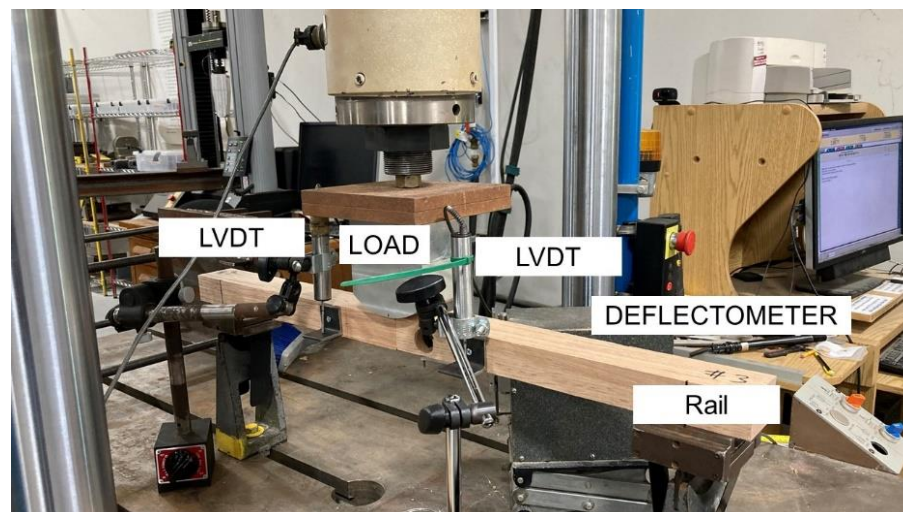


Fig. 8. Red oak rail in center-point bending setup

The bending strength capacity of the rail-to-rail joint was evaluated by center point loading bending tests. ASTM D 143 was used as a reference for the static bending testing. The static bending tests were used to estimate the maximum bending strength capacity and bending strength stiffness of a rail-to-rail fastener connector system. Figure 8 shows a red oak rail-to-rail connection system in the center point bending test setup. The span-to-depth ratio for the testing was 18-to-1 (1.375" depth and 24.75" loading span). The test loading rate was 0.5 in/min. The loading head used for the loading simulated a person's hand pushing outward against the rail.

Statistical Analysis

The effects of joint configuration on the yield moment, yield rotation, maximum moment, ductility, initial stiffness, rail deflection, shear strength, and bending loading were analyzed using SAS version 9.4. Assumptions of normality and homogeneity of variance were tested on the raw data using the Shapiro-Wilk test and Levene's test at $\alpha=0.05$, respectively.

If the assumptions of normality and homogeneity of variance were not met, then the raw data were normalized by logarithmic transformation, *i.e.* $\log(x)$, and retested again for normality and homogeneity of variance. The Kruskal-Wallis H test, a non-parametric equivalent of ANOVA (analysis of variance), was used to analyze the significance of the main effects if data could not be normalized after transformation. If the main effects proved to be significant, then Dunn's pairwise test for multiple comparisons was used to compare observation groups. If assumptions of normality and homogeneity of variance were satisfied, a one-way ANOVA and the Tukey Honestly Significant Difference (HSD) test was performed for mean separation within the main effects. If the assumption of normality was satisfied, but not the homogeneity of variance, a one-way ANOVA and the Games-Howell test were performed for mean separation within the main effects.

RESULTS AND DISCUSSION

Post-To-Rail

Static loading

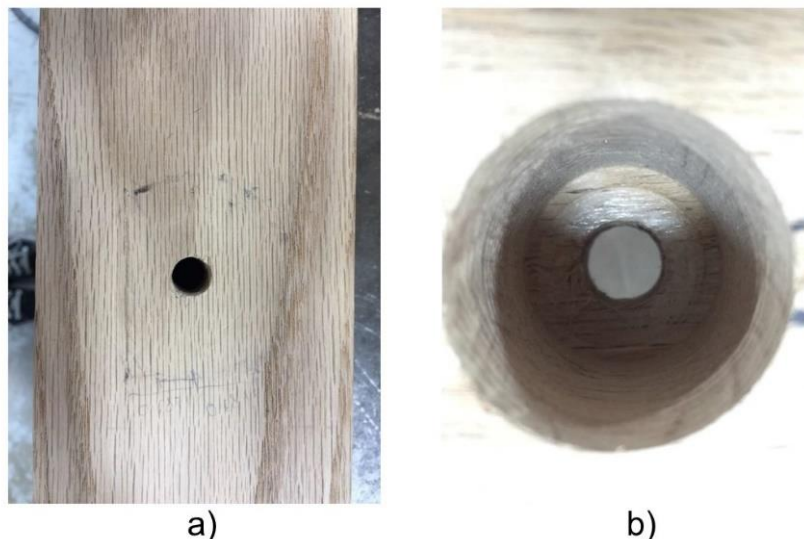
Table 1 presents the results for the static loading. The mean initial rotational modulus stiffness of rail-post fastener #301 was measured to be greater than the mean initial rotational modulus stiffness of the rail-bolt fastener #302. A 3/8" lag screw for #301 specimens was in full contact with a rail member, while a gap was formed between the 7/16" (diameter) clearance hole of the post member. For the #302 specimens, a gap was formed between the 3/8" (diameter) clearance hole of the rail and the 5/16" (diameter) hanger bolt. It was determined that the hole drilled into the end grain of the rail for the rail-bolt fastener #302 allowed for more lateral movement of the bolt within the hole during testing.

The decrease in stiffness, when compared to rail-post fastener #301, could potentially be attributed to the lateral movement occurring within the hole. This phenomenon may clarify the observed reduction in stiffness. Dong *et al.* (2021) conducted a study that revealed how connections employing dowel fasteners with excessively large predrilled holes exhibited notably diminished initial stiffness.

Table 1. Rotational Resistance Performance Parameters Descriptive Statistics for #301(C1) and #302 (C2) Connection Systems under Static Loads

		N	Mean	SD	CV(%)	Min	Max
Maximum Moment (in-lb)	C1	5	1,245	158	12.7	1,066	1,477
	C2	5	1,462	132	9.0	1,292	1,621
Rotation at Maximum Moment (radians)	C1	5	0.249	0.100	40.2	0.089	0.351
	C2	5	0.266	0.085	32.0	0.177	0.394
Yield Moment (in-lb)	C1	5	785	123	15.7	576	899
	C2	5	976	103	10.6	847	1,111
Yield Rotation (radians)	C1	5	0.017	0.003	18.1	0.013	0.020
	C2	5	0.038	0.008	21.5	0.026	0.047
Initial Stiffness (in-lb/radians)	C1	5	43,643	7,336	16.8	34,797	50,427
	C2	5	23,355	5,457	23.4	18,765	31,607

The failure mode of rail-post fastener #301 was observed to involve compression in the side grain of the post. This compression occurred both from the rail itself and due to the washer on the bolt, which also compressed into the side grain of the post (Figs. 9a and 9b). According to the wood handbook (FPL 2021) the compression strength of red oak perpendicular to the grain is 870 psi at a 12% moisture content. Given that rail-post fastener #301 is positioned at the center of the rail, the upper part of the rail experiences tension while the lower part undergoes compression. The area of the rail under the lower side of the connection measured 1.375 in². Assuming the average maximum moment for the rail-post fastener #301 is 1,200 in-lb. (100 pounds * 12 in.), the compression stress at the post would be approximately 872 psi (1,200 lb. / 1.375 in²). Notably, this value closely aligns with the published compression strength of red oak perpendicular to the grain (FPL 2021). The area of the washer within the post was measured as 0.3973 in². If the average maximum moment is 1,200 in-lb., then the compression stress in the post at the washer would be approximately 3,020 psi. This stress exceeds the published compression stress perpendicular to the grain of red oak by approximately 3.5 times. This disparity in stress levels explains the compression-induced failure of the wood under the washer within the post.

**Fig. 9.** Perpendicular-to-grain compression failure examples for #301 (C1) post members in contact with a) rail member and b) lag screw washer

The mode of failure for the rail-bolt fastener #302 connector involved the compression of the serrated nut into the plastic washer in the rail and compression in the side grain of the post (Figs. 10a and 10b). The compression stress experienced by the post would be identical to that of rail-post fastener #301, assuming the same average maximum moment of 1200 in-lb. Although the washer was constructed from plastic, the specific type of plastic was unspecified by the manufacturer. The area where the serrated nut compresses against the plastic washer within the rail was measured to be 0.286 in². Assuming the average maximum moment remains at 1,200 in-lb., the compression stress in the rail at the washer location would amount to 4,196 psi. The compression yield strength of some plastics is less than 4,196 psi (high-density polyethylene (HDPE) (2,900 psi)) (Mittal 2022).

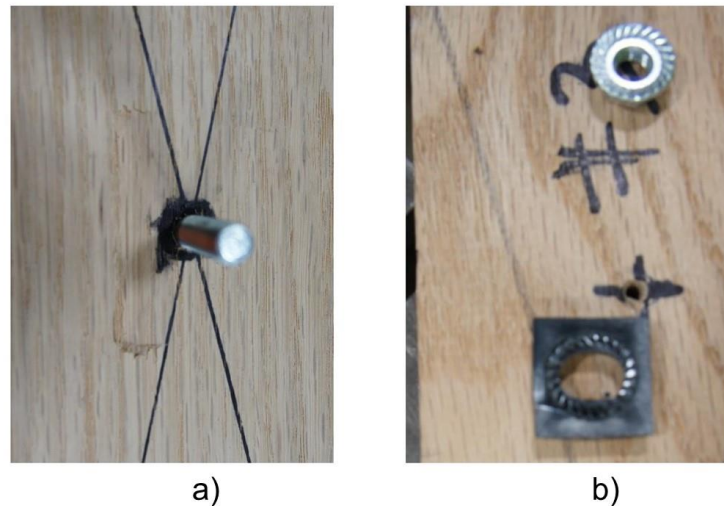


Fig. 10. Perpendicular-to-grain compression failure examples for #302 (C2) post members in contact with (a) rail member (b) hanger bolt washer

Figure 11 shows a cut-away view of the lag screw (rail-post fastener #301) on the rail member and the hanger bolt (rail-bolt fastener #302) on the post member. No noticeable withdrawal from either of the connections was observed within the wooden members. The withdrawal strength of a lag screw is dependent upon factors such as the penetration depth, lag screw diameter, grain orientation, and wood density.

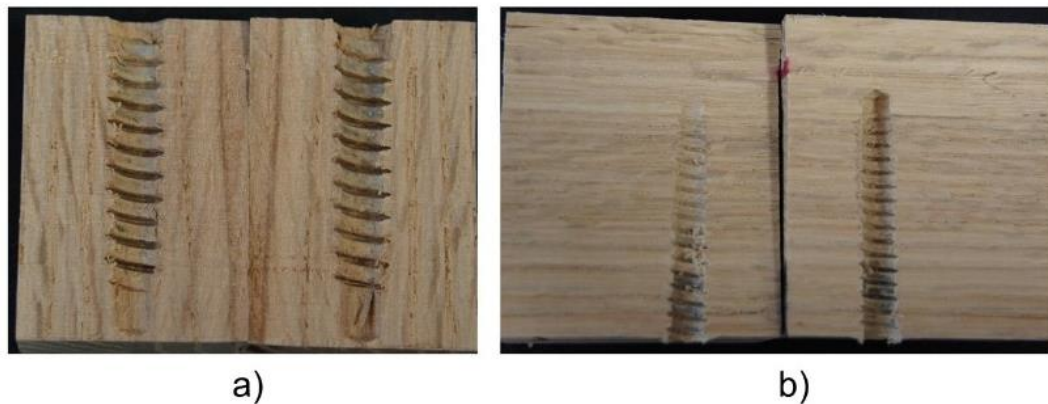


Fig. 11. Cut views of (a) #301 (C1) connection specimen's rail member (b) #302 (C2) connection specimen's post member, where a lag screw and hanger bolt were driven, respectively

Monotonic loading

Table 2 presents the results for the monotonic loading for the two connection systems. The modes of failure for the monotonic loading were consistent with the modes of failure described in the static loading section. One of the specimens (C2-M5) experienced a split rail as the mode of failure. For the yield moment, yield rotation, and maximum moment, a one-way ANOVA was used to compare the two joint configurations, since the datasets passed the normality and homogeneity of variance tests. The one-way ANOVA revealed no significant difference between the yield moment ($p=0.0512$) (Fig. 12), and the max moment ($p=0.1182$) (Fig. 13) for the two joint configurations. The one-way ANOVA revealed a significant difference between the yield rotation ($p=0.0025$) (Fig. 14) for the two joint configurations, with configuration #302 exhibiting a greater yield rotation value. To assess ductility, a one-way ANOVA was employed to compare mean \log_{10} ductility values between the two joint configurations, as the transformed datasets fulfilled the criteria of passing normality and equality of variance tests. A one-way ANOVA revealed that there was a statistically significant difference between \log_{10} ductility ($p=0.0028$) (Fig. 15) values between the two joint configurations with configuration #301 being more ductile than configuration #302. If one were to assume that the data were normal and the equality of variance without the log transformation, then the one-way ANOVA revealed the same results of a significant difference between ductility ($p=0.0142$) with configuration #301 being more ductile than configuration #302. For the initial stiffness, the median initial stiffness ranks for the two joint configurations were tested using the Kruskal-Wallis H test, since the data could not be normalized even after transformation. Pairwise comparisons using Dunn's post hoc test indicated that the median initial stiffness of configuration #301 was significantly higher than configuration #302 ($p=0.0011$) (Fig. 16). If one were to assume that the initial stiffness data were normal and with the assumption of equality of variance, the one-way ANOVA revealed the same results of the initial stiffness as the Kruskal-Wallis H test, being significantly different between the two joint configurations ($p=0.0011$).

Table 2. Rotational Resistance Performance Parameters Descriptive Statistics for #301 (C1) and #302 (C2) Connection Systems under Monotonic Loads

		N	Mean	SD	CV(%)	Min	Max
Initial Stiffness (lb-in / radians)	C1	5	50,776	8,693	17.1	39,203	59,216
	C2	5	26,914	6,245	23.2	23,243	37,982
Yield Moment (lb-in)	C1	5	742	164	22.1	461	873
	C2	5	963	141	14.6	774	1,153
Yield Rotation (radians)	C1	5	0.0142	0.0041	29.1	0.00765	0.0186
	C2	5	0.0359	0.0104	29.0	0.0188	0.0457
Maximum Moment (lb-in)	C1	5	1,182	173	14.6	904	1,353
	C2	5	1,349	126	9.3	1,234	1,498
Ductility	C1	5	11.61	4.63	39.9	8.06	19.61
	C2	5	4.61	1.92	41.7	3.28	7.98

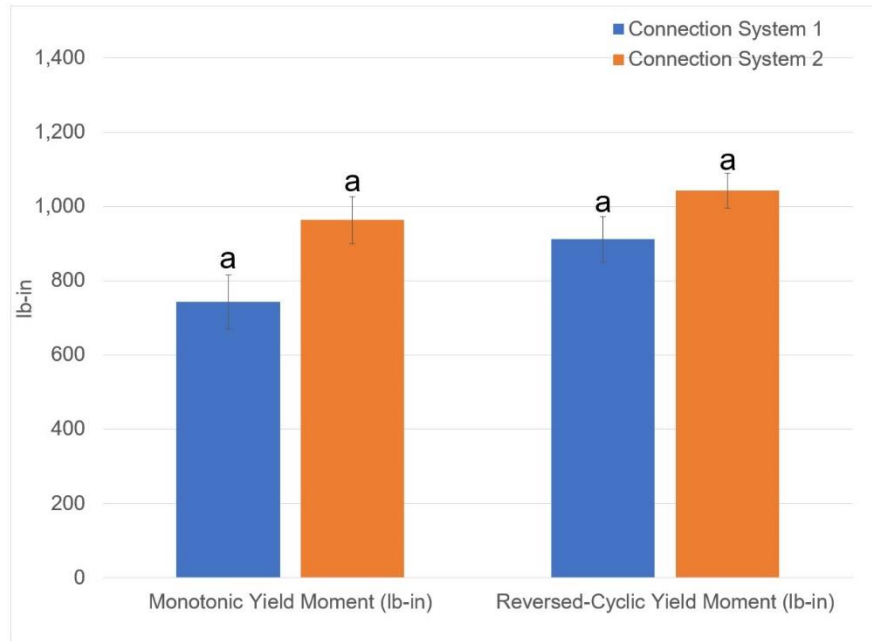


Fig. 12. Mean yield moment of the #301 (C1) and #302 (C2) connection systems under monotonic and reverse-cyclic loads (bars represent standard deviation; different letters above the bars indicate significant differences ($p < 0.05$) among connection systems within a loading condition. Tukey Honestly Significant Difference (HSD) Test for multiple comparisons found the mean values of yield moment were not significantly different between the two joint configurations.

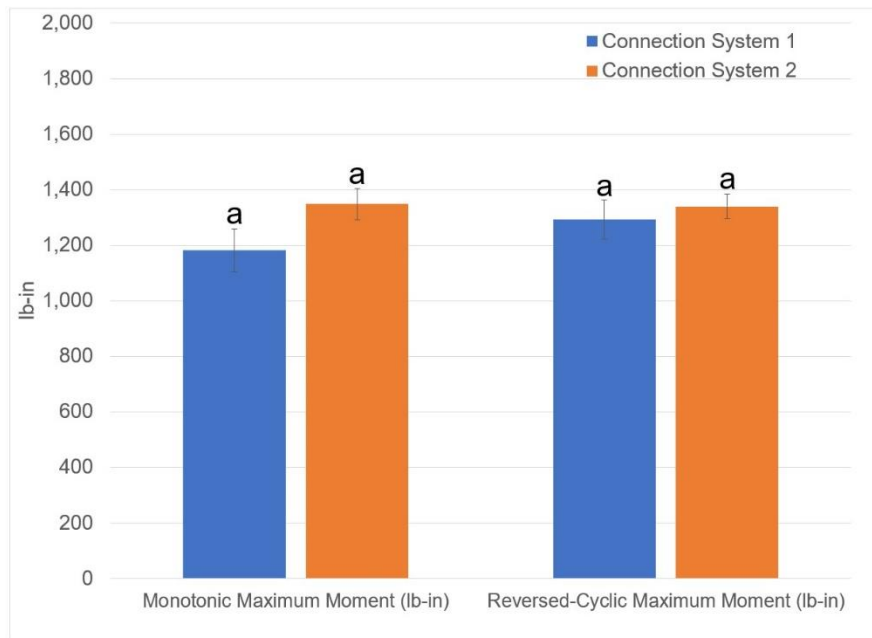


Fig. 13. Mean maximum moment of the #301 (C1) and #302 (C2) connection system under monotonic and reverse-cyclic loads (bars represent standard deviation; different letters above the bars indicate significant differences ($p < 0.05$) among connection systems within a loading condition. Tukey HSD Test for multiple comparisons found that the mean values of the maximum moment were not significantly different between the two joint configurations

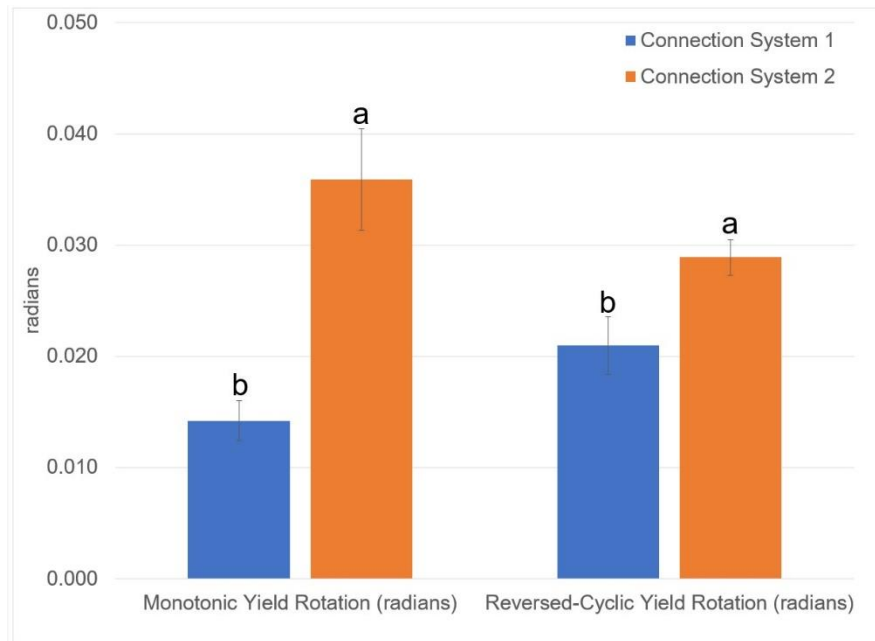


Fig. 14. Mean yield rotation of the #301 (C1) and #302 (C2) connection system under monotonic and reverse-cyclic loads (bars represent standard deviation; different letters above the bars indicate significant differences ($p < 0.05$) among connection systems within a loading condition. Tukey HSD Test for multiple comparisons found that the mean values of yield rotation were significantly different between the two joint configurations

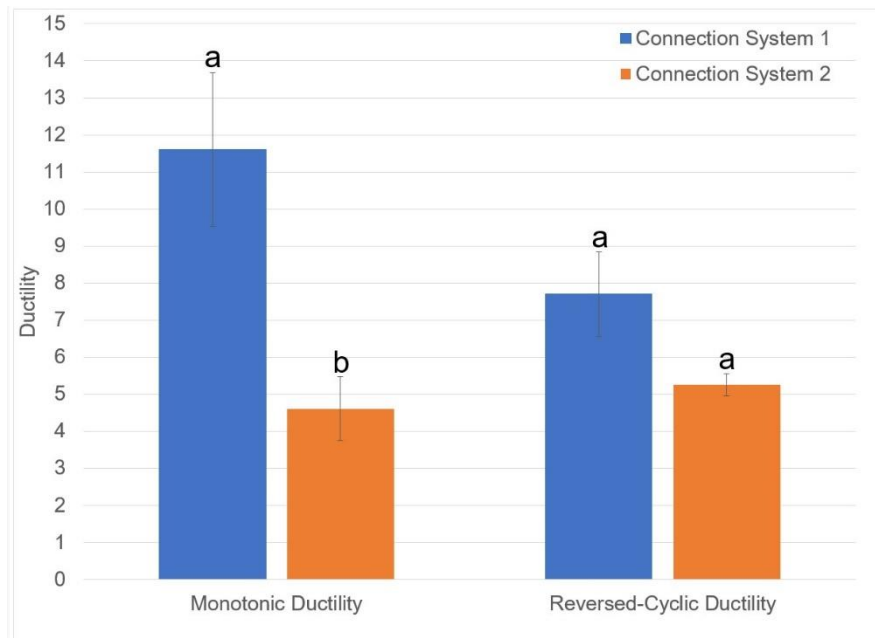


Fig. 15. Mean ductility of the #301 (C1) and #302 (C2) connection system under monotonic and reverse-cyclic loads (bars represent standard deviation; different letters above the bars indicate significant differences ($p < 0.05$) among connection systems within a loading condition. Tukey HSD Test for multiple comparisons found that the mean values of ductility for the two configurations were significantly different for the monotonic loading, but not significantly different for the reversed-cyclic loading.

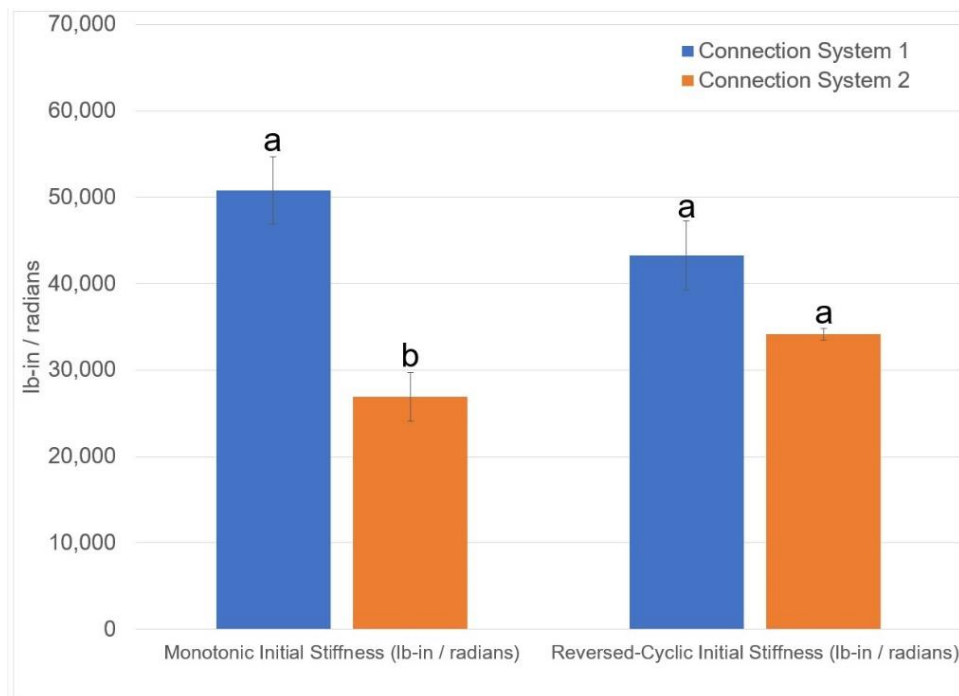


Fig. 16. Mean initial stiffness of the #301 (C1) and #302 (C2) connection system under monotonic and reverse-cyclic loads (bars represent standard deviation; different letters above the bars indicate significant differences ($p < 0.05$) among connection systems within a loading condition. Dunn's test with p -values adjusted by Bonferroni correction was used for the mean pairwise comparison.

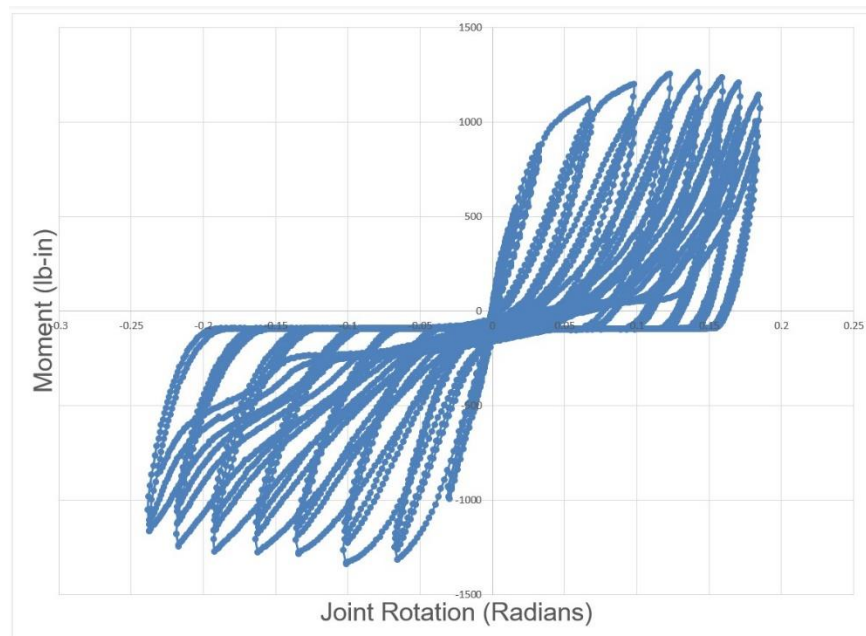
Reversed-cyclic loading

Table 3 presents the results for the reversed-cyclic loading for the two connection systems. The modes of failure for the reversed-cyclic loading were consistent with the modes of failure described in the static loading section. For the yield moment, yield rotation, maximum moment, and ductility, a one-way ANOVA was used to compare the two joint configurations, since the datasets passed the normality and equality of variance tests. The one-way ANOVA revealed no significant difference between the yield moment ($p=0.1276$) (Fig. 12), the maximum moment ($p=0.5707$) (Fig. 13), and ductility ($p=0.0731$) (Fig. 15) for the two joint configurations. The one-way ANOVA revealed a significant difference between the yield rotation ($p=0.0315$) (Fig. 14) of the two joint configurations with configuration #302 measuring a significantly higher yield rotation. For the initial stiffness, the median initial stiffness ranks for the two joint configurations was tested using the Kruskal-Wallis H test, since the data could not pass the equality of variance tests even after transformation. Pairwise comparisons using Dunn's post hoc test indicated that there was no significant difference between the median initial stiffness of the two joint configurations ($p=0.0758$) (Fig. 16).

If one were to assume as in the monotonic loading case that the initial stiffness data was normal and with the assumption of equality of variance, the one-way ANOVA revealed the same results for the initial stiffness as the Kruskal-Wallis H test being no significant difference between the joint configurations ($p=0.0528$). Figure 17 shows a typical hysteresis curve for the reversed-cyclic loading.

Table 3. Rotational Resistance Performance Parameters Descriptive Statistics for #301 (C1) and #302 (C2) Connection Systems under Reversed-cyclic Loads

		N	Mean	SD	CV(%)	Min	Max
Initial Stiffness (lb-in / radians)	C1	5	43,288	8,865	20.5	34,398	54,755
	C2	5	34,135	1,456	4.3	32,581	35,905
Yield Moment (lb-in)	C1	5	911	138	15.1	715	1,035
	C2	5	1,042	105	10.0	903	1,183
Yield Rotation (radians)	C1	5	0.021	0.0058	27.4	0.0126	0.0278
	C2	5	0.0289	0.0036	12.3	0.0245	0.0323
Maximum Moment (lb-in)	C1	5	1,292	157	12.2	1,124	1,469
	C2	5	1,340	96	7.1	1,192	1,446
Ductility	C1	5	7.70	2.55	33.1	5.4	11.9
	C2	5	5.26	0.67	12.8	4.64	6.12

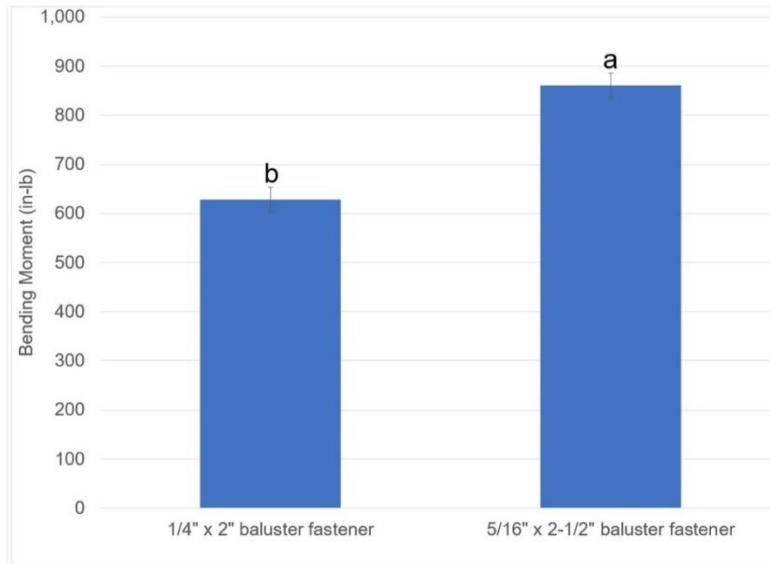
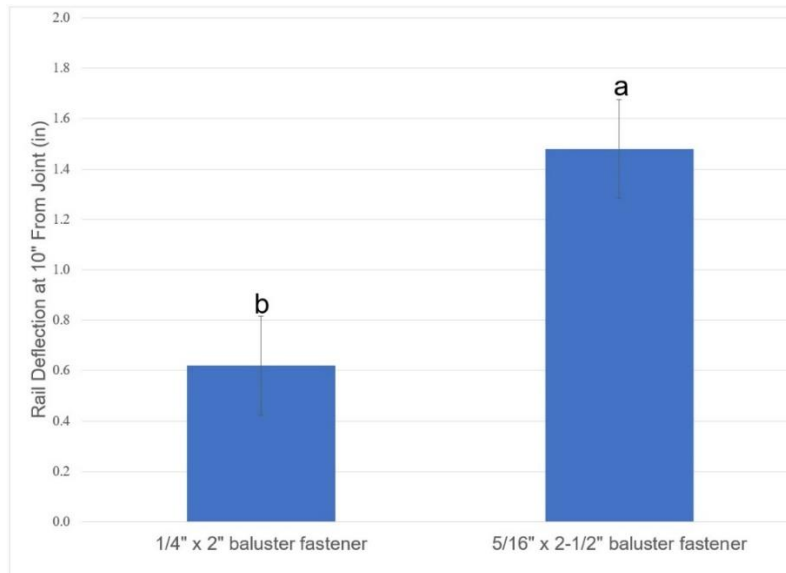
**Fig. 17.** Example of a typical hysteresis curve for the reversed-cyclic loading.

Infill(baluster)-to-Footing

Table 4 shows the maximum bending moment capacity of twenty infill-to-footing joints evaluated by cantilever bending tests. The joint deflection measurements were taken from the wire string potentiometer located 10" from the joint. The average bending moment capacity for the joints connected with the 1/4" x 2" baluster fastener was 629 in-lb with an average maximum baluster deflection of 0.62" at 10". The average bending moment capacity for the joints connected with the 5/16" x 2-1/2" baluster fastener was 861 in-lb with an average maximum baluster deflection of 1.48" at 10". For the maximum moment capacity and the rail deflection at 10" from the joint, a one-way ANOVA was used to compare the two joint configurations since the datasets passed the normality, but failed to pass the homogeneity of variance tests. The one-way ANOVA revealed a significant difference between the maximum moment ($p=0.0002$) (Fig. 18) and the rail deflection ($p=0.0004$) (Fig. 19) for the two joint configurations. The dominant modes of failure were wood compression on the footing (tread) and splitting on the infill (baluster) (Fig. 20).

Table 4. Mean Maximum Bending Moment along with Baluster Deflection at 10" from Footing (tread)

Property	Fastener Size	N	Mean	SD	CV (%)	Min	Max
Maximum Moment (in-lb)	1/4" x 2"	10	628.8	78.6	12.5	533	768
	5/16" x 2-1/2"	10	861.0	145.4	16.9	648	1,112
Baluster Deflection at Maximum Moment (in)	1/4" x 2"	10	0.62	0.24	38.9	0.34	1.2
	5/16" x 2-1/2"	10	1.48	0.62	41.9	0.72	2.64

**Fig. 18.** Mean bending moment of 1/4" x 2" baluster fastener and 5/16" x 2-1/2" baluster fastener (bars represent standard deviation; different letters above the bars indicate significant differences ($p < 0.05$). Games Howell Test for multiple comparisons found that the mean values of bending moment were significantly different between the two joint configurations.**Fig. 19.** Mean baluster rail deflection at 10" from the joint of 1/4" x 2" baluster fastener and 5/16" x 2-1/2" baluster fastener (bars represent standard deviation; different letters above the bars indicate significant differences ($p < 0.05$). Games Howell Test for multiple comparisons found that the mean values of baluster deflection were significantly different between the two joint configurations.

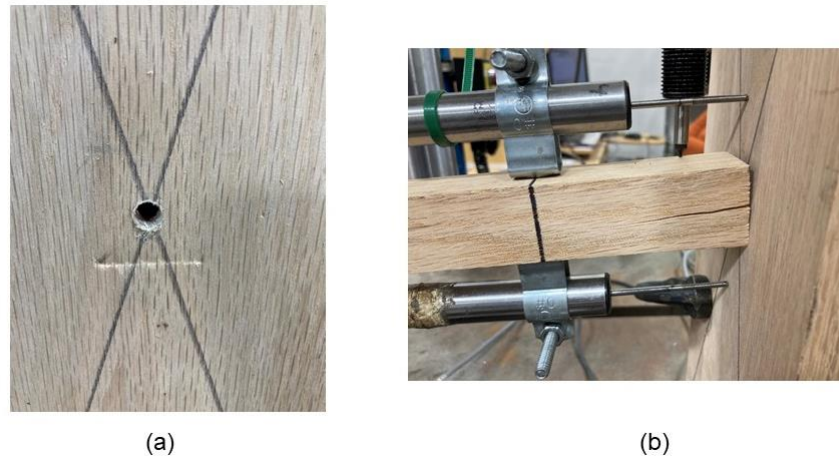


Fig. 20. (a) Wood compression on tread(footing) by infill (b) splitting in the infill

Infill(baluster)-to-Rail

Table 5 shows the measured shearing strength from the testing process. The mean value in Table 5 represents the maximum load when the samples were loaded so that both infill-to-rail connections were tested in shear. To estimate the shear strength at a single joint, the values recorded in Table 5 were divided by two. The samples with the PVAC exhibited notably higher shear strengths of 2,099 pounds and 2,307 pounds, respectively. Comparatively, samples secured with 1-1/2" finish nails demonstrated slightly greater shear strength compared to those fastened with 1-1/4" finish nails, registering values of 841 pounds and 744 pounds, respectively. For the shearing strength, a one-way ANOVA was used to compare the four joint configurations, since the datasets passed the normality test. The Games Howell separation of means procedure was used for the comparison of means because the data failed to pass the homogeneity of variance test. The homogeneity of variance test had a p-value of 0.0372. The one-way ANOVA revealed a significant difference between the shear strength of the joint configurations ($p=0.0004$). The Games-Howell for multiple comparisons showed that the configurations with the PVAC had significantly higher shear strength than the configurations without glue. The finish nail length seemed to not have any effect on the shearing strength (Fig. 21). In cases where glue was not utilized, the prevailing mode of failure was the yielding of the finish nail. Conversely, joints that incorporated glue predominantly experienced failure through the splitting of the baluster (Fig. 22). Figure 23 shows load displacement curves of a finish nail joint and a finish nail joint with PVAC adhesive. The joints with the adhesive were a lot stronger, but more brittle than the joints without the adhesive. The joints with just the finish nails were weaker, but were more ductile than the joints with the adhesive.

Table 5. Mean Maximum Double Shear Strength

Property	Configuration	N	Mean	SD	CV (%)	Min	Max
Shear Strength (pounds) two sides	1-1/4" finish nail with no glue	5	744	227	31	393	993
	1-1/4" finish nail with PVAC glue	5	2,099	1,012	44	1,238	3,407
	1-1/2" finish nail with no glue	5	841	100	12	711	929
	1-1/2" finish nail with PVAC glue	5	2,307	712	31	1,259	3,059

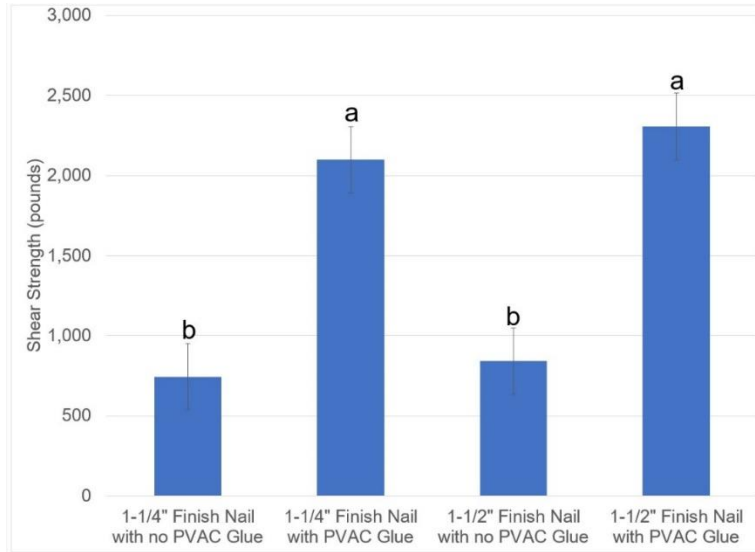


Fig. 21. Mean shear strength of infill-to-rail configurations (bars represent standard deviation; different letters above the bars indicate significant differences ($p < 0.05$). Games-Howell Test for multiple comparisons found that the mean shear strength values were significantly different between the configurations with PVAC glue and configurations without PVAC glue.

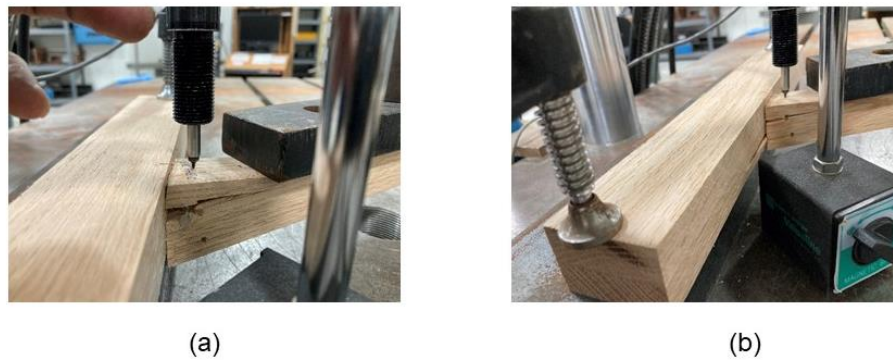


Fig. 22. Examples of splitting on the infill(baluster) (a) and (b)

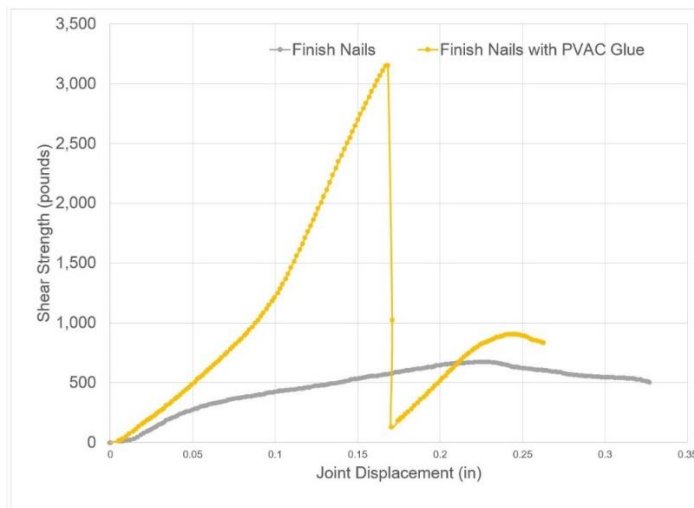


Fig. 23. Example shear strength displacement curves of a joint with finish nails and a joint with finish nails with PVAC glue

Rail-to-Rail

Table 6 shows the maximum bending strength measurements for the tested joints. The joint deflection measurements taken from the movement of the load head are also shown. The average measured bending strength was 246 pounds with an average joint deflection of 1.17” for the rail-bolt #302 fastener According to American Society of Civil Engineers ASCE/SEI 7-10 – Minimum Design Loads for Buildings and other Structures states that a handrail should be able to resist a single concentrated load of 200 pounds applied in any direction or resist a force of 50 pounds / linear feet. If using a support span of 24.75”, the present test results passed the 50 pounds / linear feet minimum. The major mode of failure for the joints was the yielding of the lag bolt. One of the joints had the rail split at the laminate glue line. The initial stiffness for all fifteen joints was similar. The behavior of the load-deflection curves was influenced by the modes of failure. The average bending strength was 1,848 pounds with an average rail deflection at mid-span of 1.04” for the solid red oak rails. The solid rails easily passed the 50 pounds / linear feet minimum mentioned and described previously. The dominant mode of failure for the solid rails was cross-grain failure. A large percentage of the red oak rails had cross grain. Since the data failed to pass the homogeneity of variance test for the bending strength and midspan deflection for the two configurations according to Levene’s test ($p=0.0029$) and ($p=0.0019$), respectively, but pass the normality test the data was analyzed using a one-way ANOVA with the Games-Howell post hoc procedure for separation of the means. The pairwise comparisons using Games-Howell post hoc test indicated that there was a significant difference between the mean bending strength of the two configurations ($p<0.0001$) (Fig. 24). The pairwise comparisons using Games-Howell post hoc test also indicated that there was no significant difference between the mean bending deflection at midspan of the two configurations ($p=0.3442$) (Fig. 25).

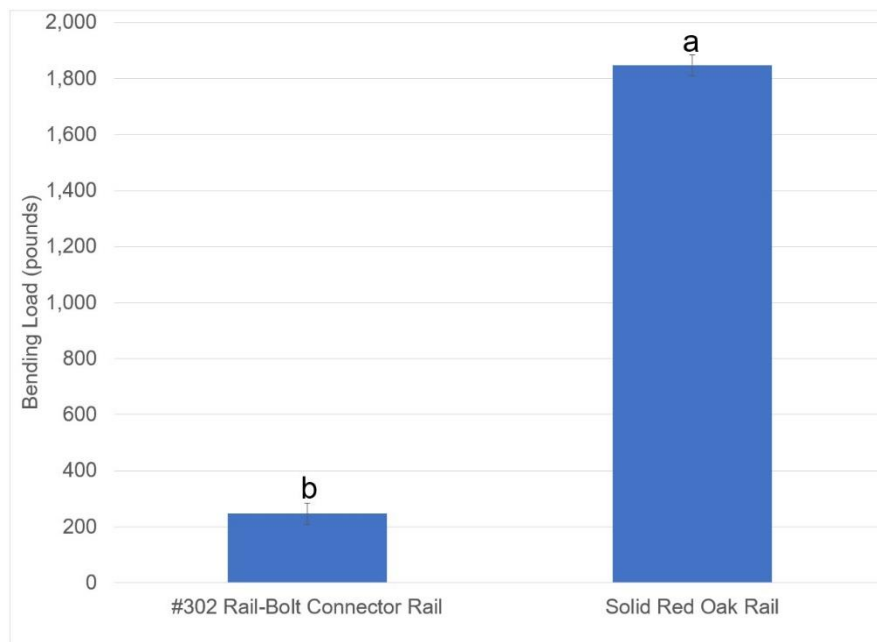


Fig. 24. Mean bending strength of rail-to-rail configurations (bars represent standard deviation; different letters above the bars indicate significant differences ($p<0.05$). Games-Howell Test for multiple comparisons found that the bending load values were significantly different between the configurations.

Table 6. Mean Maximum Bending Strength along Load Head Movement at Center

Property	Fastener Size	N	Mean	SD	CV (%)	Min	Max
Maximum Bending Strength (lb)	Rail-Bolt #302	15	246	31	12.6	196	311
	Solid Rail	15	1,848	260	14.1	1,342	2,277
Joint Deflection at Maximum Bending Strength (in)	Rail-Bolt #302	15	1.17	0.48	41.5	0.42	1.93
	Solid Rail	15	1.04	0.18	17.6	0.71	1.32

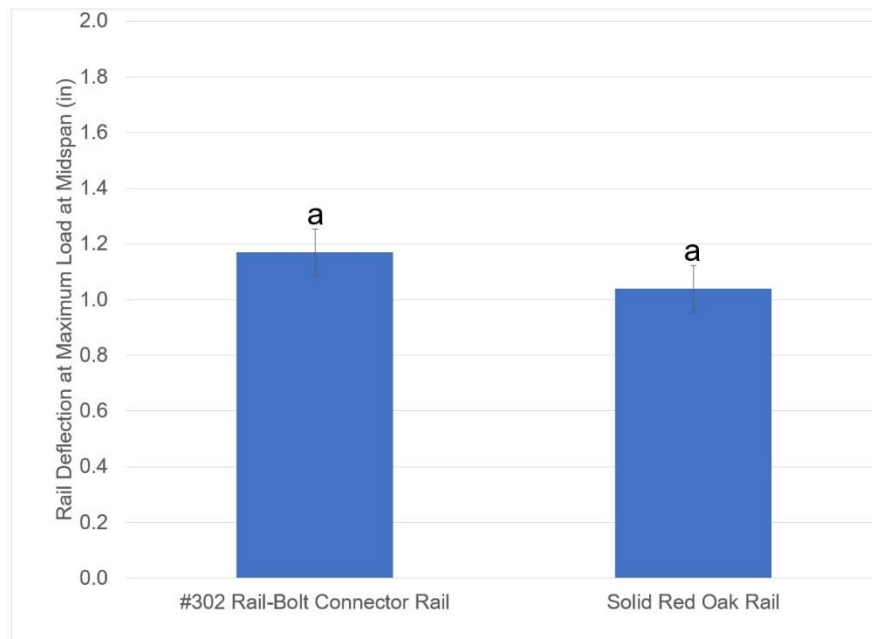


Fig. 25. Mean rail deflection of rail-to-rail configurations (bars represent standard deviation; different letters above the bars indicate significant differences ($p < 0.05$). Games-Howell Test for multiple comparisons found that the deflection values were not significantly different between the configurations.

CONCLUSIONS

1. This study examined the monotonic and cyclic behavior of the moment-resisting performance of two different types of concealed single-bolt connectors linking the post-to-handrail of a stairway guard system. The main components of the two systems were a 3/8" lag screw and a 5/16" hanger bolt. The joint with the 3/8" lag screw measured a higher initial stiffness than the 5/16" hanger bolt joint, but it was only significantly higher statistically for the monotonic loading condition. There was no significant difference in the yield strength of the joints regardless of the loading conditions (monotonic or reversed-cyclic), but the yield rotation was significantly more for the 5/16" hanger bolt for both loading conditions. The modes of failure were similar for both joints being compression of the wood on the post and the rail.

2. This study examined two infill(baluster)-to-rail connections. Both connection systems measured average loads higher than required by the International Building Code (IBC) for balusters.
3. This study examined four infill(baluster)-to-rail configurations. The mode of failure was the splitting of the baluster when using PVAC glue. The glue joints measured higher shearing values than the joints with no PVAC glue. The finish nail lengths had no significant influence on the shearing strength even though the longer nails measured a slightly higher mean shearing strength.
4. This study examined two rail-to-rail configurations. Both the rail-to-rail configurations passed the requirements of being about to sustain a load of 50 pounds / linear feet as proposed in the American Society of Civil Engineers ASCE/SEI 7-10.

ACKNOWLEDGMENTS

This research was conducted in cooperation with the USDA Forest Service Forest Products Laboratory (FPL). This institution is an equal opportunity provider. This publication is a contribution of the Forest and Wildlife Research Center, Mississippi State University. This paper was approved as journal article SB1121 of the Forest & Wildlife Research Center, Mississippi State University and was received for publication in November 2023.

REFERENCES CITED

- ASCE 7-05/ANSI A58 (2005). "Minimum design loads for buildings and other structures," American Society of Civil Engineers (ASCE), Reston, VA.
- ASTM E 2126 (2019). "Standard test methods for cyclic (reversed) load test for shear resistance of vertical elements of the lateral force resisting systems for buildings," ASTM International, West Conshohocken, PA.
- ASTM D 4442 (2020). "Standard test methods for direct moisture content measurement of wood and wood-based materials," ASTM International, West Conshohocken, PA.
- Bauchau, O. A., and Craig, J. I. (2009). *Euler-Bernoulli Beam Theory. Structural Analysis. Solid Mechanics and Its Applications*. Vol 163. Springer, Dordrecht.
- Dong, W., Li, M., He, M., and Li, Z. (2021). "Experimental testing and analytical modeling of glulam moment connections with self-drilling dowels," *Journal of Structural Engineering* 147(5), 1-7. DOI: 10.1061/(ASCE)ST.1943-541X.000297
- EN 26891 (1991). "Timber structures, joints made with mechanical fasteners, general principles for the determination of strength and deformation characteristics," European Committee for Standardization (CEN), Brussels, Belgium.
- EN 12512/A1 (2005). "Timber structures, test methods, cyclic testing of joints made with mechanical fasteners," European Committee for Standardization (CEN) Brussels, Belgium.
- Forest Products Laboratory (FPL) (2021). *Wood Handbook – Wood as Engineering Material*, USDA Forest Service, Madison, WI.
- Maki, B. E. (1985). *Influence of Handrail Shape, Size and Surface Texture on the Ability of Young and Elderly Users to Generate Stabilizing Forces and Moments* (Technical

- Report Number 29401), National Research Council of Canada, Ottawa.
- Mittal, A. (2022). “What is compressive strength of plastics,” (https://plasticranger.com/what-is-compressive-strength-of-plastics-the-complete-guide/#Difference_Between_Compressive_Strength_and_Compressive_Modulus), Accessed 31 January 2023).
- Pencik, J. (2015). “Analysis of support of stairs in a wooden prefabricated staircase with one-sided suspended stairs made from Scots pine (*Pinus sylvestris*) with the use of experimental tests and numerical analysis,” *Wood Research* 60(3), 477-490.
- Pousette, A. (2006). “Testing and modeling of the behavior of wooden stairs and stair joints,” *Journal of Wood Science* 52, 358-362. DOI: 10.1007/s10086-005-0778-8
- SAS Institute (2016). *SAS Software, Version 9.4*, The SAS Institute Inc., Cary, NC, USA.
- Templer, J., Archea, J., and Cohen, H. H. (1985). “Study of factors associated with risk of work-related stairway falls,” *Journal of Safety Research* 16(4), 183-196. DOI: 10.1016/0022-4375(85)90005-2
- Wynne, D., Hampton, S., Cregger, N., and Suits, C. (2000). *Coffman Stair Building Guide*, Coffman Stairs, Marion, VA, USA.

Article submitted: November 8, 2023; Peer review completed: December 2, 2023;
Revised version received and accepted: January 3, 2024; Published: January 10, 2024.
DOI: 10.15376/biores.19.1.1410-1432